Memoirs of the Faculty of Engineering, Okayama University, Vol. 43, pp. 8-15, January 2009

Dispersion Models and Electromagnetic FDTD Analyses of Nanostructured Metamaterials using Parallel Computer

Ryosuke UMEDA, Chieko TOTSUJI,
Kenji TSURUTA*, Hiroo TOTSUJI
Graduate School of Natural Science and Technology
Okayama University
Okayama 700-8530, Japan

(Received December 1, 2008)

Metamaterial which has negative permittivity and permeability is investigated via computer simulations. Effects of the nanostructure on dielectric and magnetic properties of the material are taken into account by introducing the Drude-Lorentz model in the materials dispersion. We include multi-band process in the dielectric response in order to reproduce accurately experimental values of bulk Au thin film. Size effect on the dispersion is examined by comparing the model with that of a noble metal particle. Based on the dispersion model constructed, we analyze the electromagnetic response of nanostructured metamaterials to evanescent waves at microwave and optical frequencies via finite-difference time-domain simulatioins on parallel computer. A re-focusing and an amplification of the evanescent waves propagating through a metamaterial, consisting of metal slab/vacuum stacking, is demonstrated for the frequencies of 30GHz and 744THz.

1. INTRODUCTION

The material which has negative permittivity and permeability simultaneously, has been called "left handed" or double-negative material (DNGM). The DNGM has negative refractive index (NRI), negative phase velocity, reversed Doppler effect and hence a magnification of the electromagnetic near-field, which leads to possible fabrication of "super lens".[1-5] Metamaterials are made artificially to have such characteristics of the DNGM. They have been demonstrated experimentally for microwave frequencies.[4] Various types of structures and materials combinations have been proposed and tested for optical frequencies.[5] Nevertheless, metamaterials operating with low energy loss for visible light have not been fabricated so far. Given that such deficiency has been improved, optical metamaterials are anticipated as novel materials used for super lens, tunneling devices, compact resonators and highly directional optical sources.

In this paper, we construct a dispersion model which satisfies the NRI at microwave and optical frequencies based on the Drude-Lorentz model with multi-band effects. Non-Drude-like response of metal to optical frequency is known to be caused either by discrete levels in electronic energy bands in the material or by its level shift due to the size effect. We analyze transmission characteristic of electromagnetic wave through metamaterials for microwave at 30GHz and an optical range at 744THz using the finite-difference time-domain (FDTD) method. The FDTD method is usually employed for numerical analyses on devices in macroscopic scale for microwave and infrared frequencies. In the present study we extend the FDTD method to optical frequencies by introducing the Drude-Lorentz dispersion function.

2. METHODOLOGY

2.1 Dispersion Model

To simulate the metamaterials with NRI, materials dispersions have to be considered at the frequency ranges interested. In the Drude dispersion model, a dielectric constant is written as

$$\epsilon(\omega) = \epsilon_0 \left(1 - \frac{\omega_p^2}{\omega(\omega + i\Gamma_D)} \right), \qquad (1)$$

where ω_p is the plasma frequency and Γ_D is the damping coefficient. The Drude model can describe dielectric properties of metals well at the near infrared range

*Email:tsuruta@elec.okayama-u.ac.jp

(200-400THz). On the other hand, it fails to reproduce the experimental spectrum at the range of visible light. This can be attributed to the fact that the standard Drude model takes only electromagnetic response of nearly-free electrons into account. Typical materials used in the experiments for DNGM are the noble metals that have non-Drude-like dispersions at optical frequencies. To overcome this drawback in the Drude model, we adopt the Drude-Lorentz (DL) model to include processes of interband transitions of electrons in metals.[6] The DL model for multi-band transitions is written as

$$\epsilon(\omega) = \epsilon_\infty - \frac{\omega_p^2}{\omega(\omega - i\Gamma_D)} - \sum_k \frac{\Delta\varepsilon_k \Omega_{kL}^2}{(\omega^2 - \Omega_{kL}^2) + i\Gamma_L \omega}, \tag{2}$$

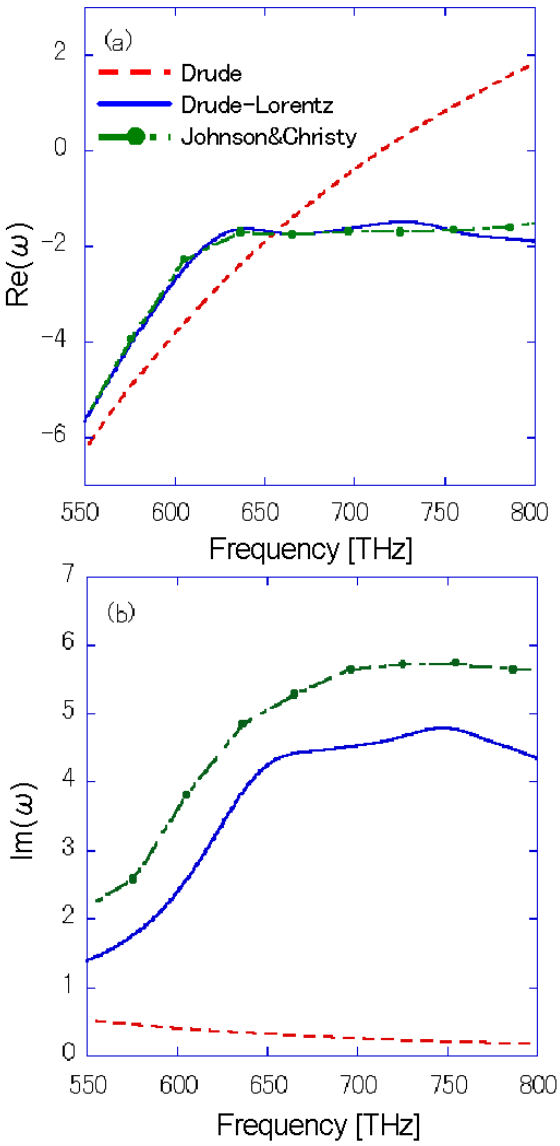

Fig. 1: **(a)** Real and **(b)** imaginary part of the permittivity of bulk Au in the Drude model and in the Drude-Lorentz model.

Table 1: Value of the parameters used in the Drude and the DL model.

	Drude	Drude-Lorentz
ϵ_∞	9.0685	5.9673
$\omega_p/2\pi$[THz]	2155.6	2113.6
$\Gamma_D/2\pi$[THz]	18.36	15.92
$\Omega_{1L}/2\pi$[THz]		650.0
$\Omega_{2L}/2\pi$[THz]		700.0
$\Omega_{3L}/2\pi$[THz]		750.0
$\Omega_{4L}/2\pi$[THz]		800.0
$\Omega_{5L}/2\pi$[THz]		850.0
$\Omega_{6L}/2\pi$[THz]		900.0
$\Omega_{7L}/2\pi$[THz]		950.0
$\Gamma_L/2\pi$[THz]		104.86
$\Delta\epsilon_1$		0.4
$\Delta\epsilon_2$		0.2
$\Delta\epsilon_3$		0.3
$\Delta\epsilon_4$		0.2
$\Delta\epsilon_5$		0.2
$\Delta\epsilon_6$		0.07
$\Delta\epsilon_7$		0.05

where Ω_{kL} is the oscillator strength of kth mode, Γ_L is the spectral width of the Lorentz oscillators, and $\Delta\epsilon_k$ is a weighting factor.

Figure 1 depicts frequency spectra of the permittivity of Au simulated by the models at terahertz and optical frequencies. Also shown are the experimental values of Au thin film measured by Johnson and Christy in 1972.[7] The permittivity modeled by the Drude function increases monotonically with respect to frequency and it changes negative to positive at 710THz. On the other hand, the DL model agrees very well with the experimental values for all frequency ranges considered. In the present model, the DL function is constructed by fitting the experimental data to seven absorption lines for interband transition. Values of the fitted parameters for the Drude and the DL model are listed in Table1. Thus, the simulated and measured curves for the dispersion are proved to be well represented by including multiband effects.

To consider further the size effect of the nanostructure on the dielectric properties, we introduce additional terms in the DL model: In the single-band transition model, the permittivity is written as

$$\epsilon_{Au} = \epsilon_{bulk} + \omega_p^2 \left(\frac{1}{\omega^2 + \gamma_\infty^2} - \frac{1}{\omega^2 + \gamma(R)^2} \right) + i\frac{\omega_p^2}{\omega} \left(\frac{\gamma(R)}{\omega^2 + \gamma(R)^2} - \frac{\gamma_\infty}{\omega^2 + \gamma_\infty^2} \right) \tag{3}$$

Table 2: Values of the parameters adoped for the size effect with the metal particle.

	size effect
v_F[m·10^6/s]	1.4
$\omega_p/2\pi$[THz]	2113.6
ϵ_{bulk}	Figure. 1
l_∞[nm]	42
γ_∞[1/s]	33.3

R[nm]	$\gamma(R)$[1/s]
2.4	616.6
3.0	500.0
4.1	374.8
4.7	331.2
5.4	292.6
7.6	217.5

where γ_∞ is the relaxation frequency in bulk material, and $\gamma(R)$ is the relaxation frequency dependent on the size of the system.[8] γ_∞ and $\gamma(R)$ are given as

$$\gamma_\infty = \frac{v_F}{l_\infty} \tag{4}$$

$$\gamma(R) = \gamma_\infty + \frac{v_F}{R} \tag{5}$$

where v_F is the Fermi velocity, l_∞ is the bulk mean free path and R is the radius of the metal particle. Table 2 represents values of the parameters adopted for the size effect in the metal particle. The effective mean free path is smaller than l_∞ in all clusters with $2R \leq l_\infty$. This is called the "free pass effect". Figure 2 shows frequency spectrum of permittivity in the DL model with and without the size effect. Both the real and the imaginary part increase as the size is smaller. In contrast, however, an experimental result reported in Ref.9 is different dependence on the system size in real part. Also, the size dependence is smaller than the effect appeared due to the multi-band transition.

2.2 **Simulation Method**

To implement these dispersion effect on the FDTD algorithm, we adopt two approaches; one is the auxiliary difference equation (ADE)[10] method and the other is recursive convolution (RC) method.[11] In the ADE method, we solve differential equations for not only the electric field and magnetic field, but also the electric and magnetic polarization in medium. In TEz mode, where only Ex, Ey and Hz vary, these are given by

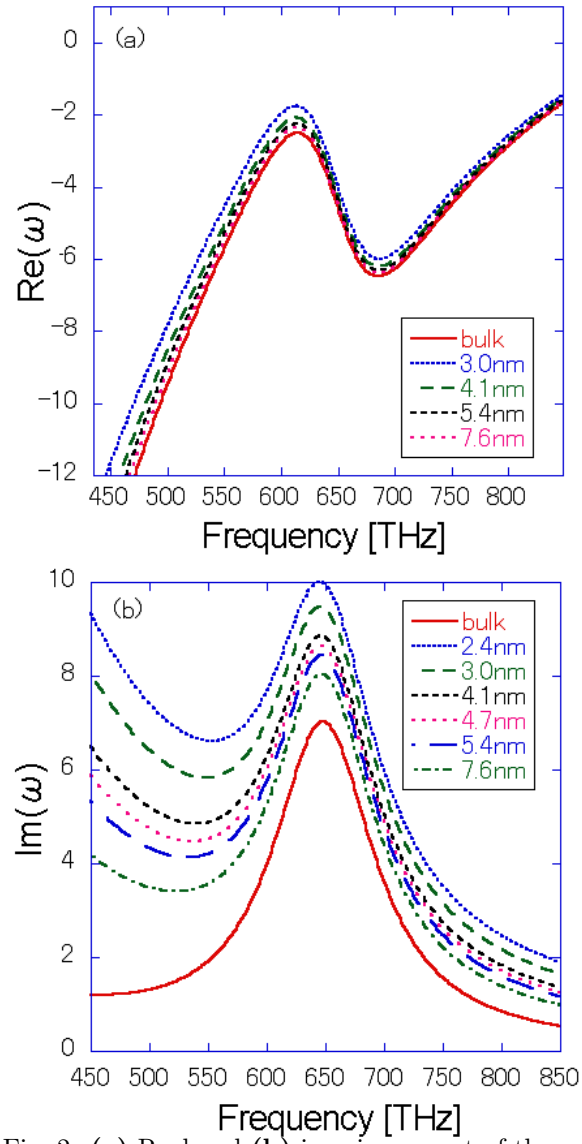

Fig. 2: **(a)** Real and **(b)** imaginary part of the permittivity in the Drude-Lorentz model with size dependence.

$$\epsilon_0\omega_p^2 Ex = \frac{\partial J_x}{\partial t} + \Gamma J_x, \tag{6}$$

$$\epsilon_0\omega_p^2 Ey = \frac{\partial J_y}{\partial t} + \Gamma J_y, \tag{7}$$

$$\mu_0\omega_p^2 Hz = \frac{\partial K_z}{\partial t} + \Gamma K_z, \tag{8}$$

where J_x and J_y are the polarization currents and K_z is the magnetic polarization current.

In the RC method, we calculate a convolution integral of electric flux density and electric field recursively. This is represented by

$$\mathbf{D}(t) = \epsilon_0\epsilon_\infty \mathbf{E} + \epsilon_0 \int_0^t \chi(\tau)\mathbf{E}(t-\tau)d\tau, \tag{9}$$

where $\mathbf{D}$ and χ are electric flux density and susceptibility, respectively, and

$$\epsilon_r(\omega) = \epsilon_\infty + \chi(\omega), \tag{10}$$

is the permittivity.

Details for the implementations of both ADE and RC method are described in APPENDIX. In the FDTD simulation with the RC method we estimate the convolution integral by approximating the electric field to be constant in the time interval Δt. Adopting the Ampere's law, the electric field at the nth time step is evolved from the $(n-1)$th step as

$$\mathbf{E}^n = \frac{\epsilon_\infty}{\epsilon_\infty + \chi^0}\mathbf{E}^{n-1} + \frac{1}{\epsilon_\infty + \chi^0}\sum_{m=0}^{n-2}\mathbf{E}^{n-1-m}\Delta\chi^m + \frac{\Delta t/\epsilon_0}{\epsilon_\infty + \chi^0}\nabla\times\mathbf{H}^{n-\frac{1}{2}}, \tag{11}$$

where χ^0 and $\Delta\chi^m$ are given by

$$\chi^0 = \int_0^{\Delta t}\chi(\tau)d\tau, \tag{12}$$

$$\Delta\chi^m = \chi^m - \chi^{m+1}. \tag{13}$$

We use the ADE method for simple model such as the Drude model at microwave frequencies whereas complicated model such as the DL model at optical frequencies is calculated by the RC method. In order to perform the FDTD simulation efficiently on parallel computer, we implement the real-space domain decomposition algorithm: At each time step, physical quantities at each grid point are calculated parallely on the assigned computing node. The CPU in each machine has four computing units (cores) operated with 2.4GHz clock. The message passing interface (MPI) is used for the internode communications. Figure 3 shows the domein-decomposition algorithm. In this algorithm the simulated space is divided into subdomains. The information, such as electric and magnetic field, at the boundary points in each subdomain is exchanged mutually between neighboring nodes at each time step in the finite difference calculation.

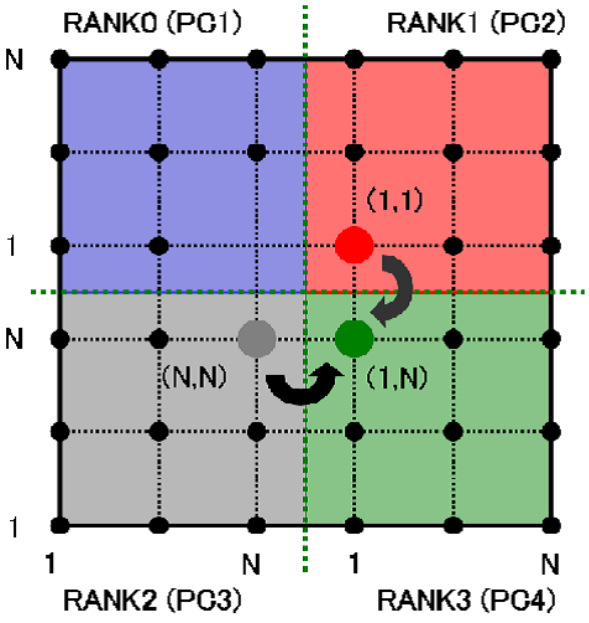

Fig. 3: Domain-decomposition algorithm.

3. RESULT

3.1 Model

In the "hyper lens", recently proposed in Ref.3, the evanescent image has to be propagated from the near field to the far field and to magnify the image size so that human's eye can observe it. Based on Ref.3, we first consider a cylindical structure of the DNGM slabs as shown Fig.4 (a). The DNGM slabs have the frequency dependent permittivity and permeability represented by the Drude or the DL model, whereas these are positive constants in the vacuum regions. The incident waves in TMz mode are propagated from the line sources.

Next, we analyze response of the DNGM slabs, as shown Fig.4 (b), to the evanescent wave at microwave frequency (30GHz) for which the refractive index of the slabs is close to -1 in the Drude model. The plane waves of TEz mode are generated in the source region. The perfect conductor with two slits is placed between the source and the DNGM slab to make the incident waves quasi-evanescent which decay rapidly along the distance from exits of the slits due to diffraction and superposition effects.[12]

We adopt periodic DNGM/vacuum stacking structures in the present model. If the slab is made of an ideal DNGM, the evanescent wave propagates without energy absorption by the slab whereas in real materials, the energy loss is inevitable due to the finite width of peaks in the imaginary part of permittivity and permeability. In this sense, thinner DNGM is better. On the other hand, if the DNGM slab is thinner than $d1$ depicted in Fig4. (c), the re-focus point is not generated. Therefore, the thickness and periodicity of the stacking have to be optimized to observe the evanescent wave propagating from the near field to the far field so that focus and re-focus points are matched at each stacking.

We analyze transmission characteristics of the evanescent waves through the system at microwave and optical frequencies via the FDTD simulations. Parameters and methods used in the present simulations are summarized in Table 3.

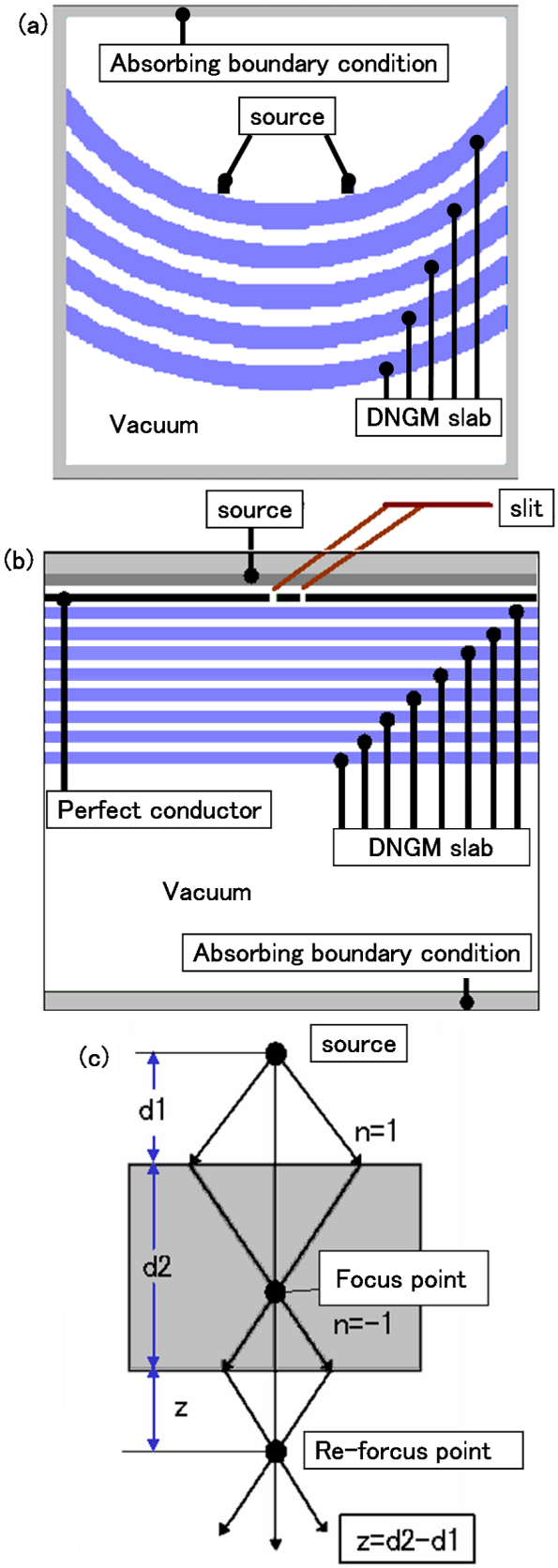

Fig. 4: **(a)**, **(b)** Model in the present FDTD analysis. **(c)** Schematics of DNGM slab with n=-1 and refocusing of image in the other side of slab.

Table 3: Summary of parameters and methods used in the FDTD simulations.

	Frequency	
	30[GHz]	744[THz]
step size	100	100
time step	20000	100000
Δx	0.1[mm]	4.03[nm]
Δt	0.98[ms]	201.5[ps]
Number of cell	4000×1000	2000×2000
Model	Drude	Drude,DL
Number of DNGM	0,5,8	1
Slit width	0.5[mm]	20[nm]
Thickness of DNGM	2.5[mm]	128[nm]
Method	ADE	RC

3.2 Analysis for Microwave Frequency

Figure 5(a) shows the intensity distributions of propagating wave Ez in the system shown Fig.4 (a). The distance of two propagating waves emitted from the line sources expands as electric field transmits through the DNGM slabs. Thus the magnification is shown to be achieved by this model.

Figure 5(b) shows the intensity distributions of evanescent wave Ey in the system shown in Fig.4 (b). ¿From Fig.5 (b), it is clear that the evanescent wave emitting from the two slits is amplified in each DNGM slab. While propagating through the periodic DNGM-/vacuum stacking structure, it repeats amplification and decay in each slab region. In Fig.5 (c), we can also see the re-focusing of the incident image at the exit of the stacking. This indicates that the sequence of the imaging and re-focusing may lead to "super lensing" that the near-field image is effectively magnified.

We also plot a cross-sectional diagram of the intensity distributions in Fig.5 (c). Solid line represents the propagation through eight layers of the DNGM slab and dotted line is for the case without the DNGM. This shows that the evanescent wave emitted in the near field transmits and propagates through the system, as if the wave is transformed to the far field.

3.3 Analysis for Optical Frequency

We also study the electromagnetic response of the DNGM slab, similar geometry analyzed in the previous section, to the waves at optical frequency. The frequency investigated is 744THz. The frequency dependence of permittivity and permeability is represented by the DL model, as described in Sec.2. We also perform the FDTD simulation with the Drude model for comparison. Figure 6 shows the propagation characteristic of electromagnetic wave through single

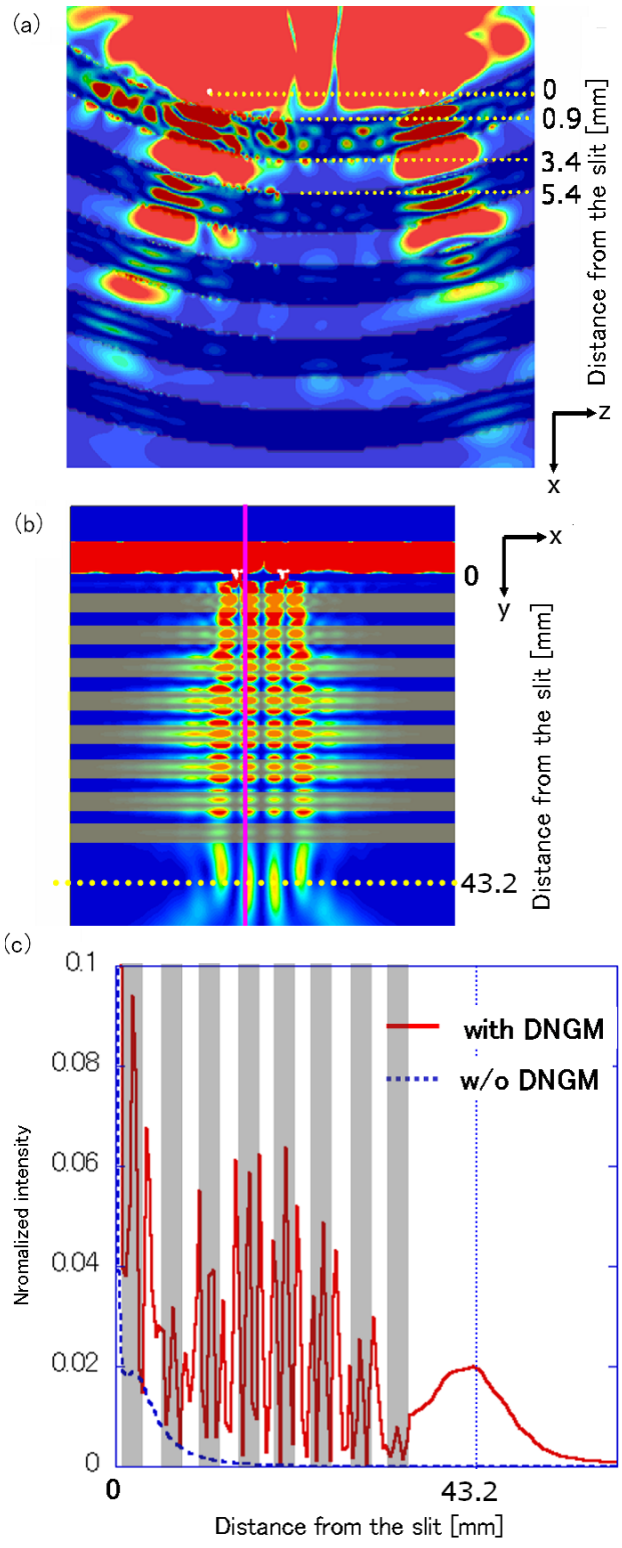

Fig. 5: **(a)**,**(b)** Normalized intensity distribution of wave propagating through the DNGM at microwave frequency. ;**(a)** propagationg wave, **(b)** evanescent wave. **(c)** The cross-sectional diagram at the vertical line in **(b)**. The solid line is the result for the DNGM stacking of eight layers and the dotted line is for vacuum.

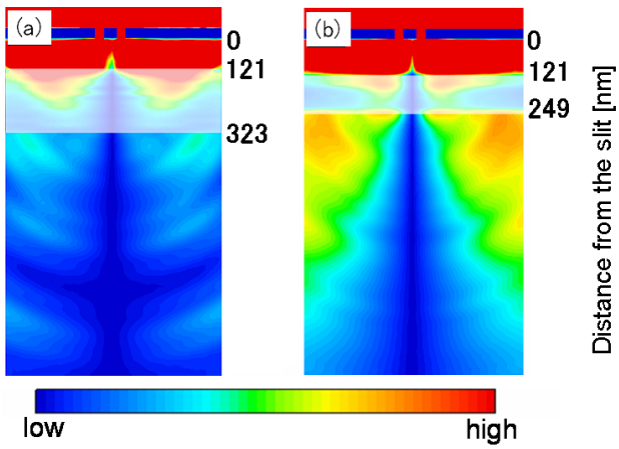

Fig. 6: Normalized intensity distributions of evanescent wave. **(a)** Drude model, and **(b)** DL model for f=744THz.

DNGM slab at 744THz. Comparisons between the results for the Drude and for the DL model are also depicted in the figure.

At the frequency of 744THz, the Drude model gives the refractive index of 0.67. Since the refractive index is positive, the DNGM behaves as a right-handed material, and hence the evanescent wave decays exponentially as shown in Fig.6 (a). On the other hand, the DL model which gives refractive index -1.57 at the frequency leads to an amplification as demonstrated in Fig.6 (b). These comparisons illustrate clearly the importance of the treatment for electromagnetic responses of the metamaterials to the waves especially in the optical frequency range.

4. CONCLUSION

We have constructed dispersion models for nanostructured metamaterials at wide-ranged frequencies. By using the DL model for the multi-band transitions, we were able to reproduce the frequency spectrum of bulk Au measured experimentally by Johnson and Christy. This improvement leads to that the DNGM has negative refractive index over the full visible spectrum. The amplification in the DNGM slab was observed at 744THz via the FDTD simulations. These results indicate that by properly treating the materials dispersion, the nanostructured metamaterials should poses the characteristics of the left-handed material in the optical frequency range.

ACKNOWLEDGEMENTS

This work was supported by Grant-in-Aid for Scientific Research on Priority Areas “Nano Materials Science for Atomic Scale Modification 47” from MEXT of Japan.

APPENDIX: Numerical implementation of the ADE and the RC method

In the ADE method, the differencial equations given by Eq. (6)-(8), where only E_x, E_y, H_z, J_x, J_y and K_z vary, are transformed as finite-difference formula and represented by

$$E_x|^{n+1}_{i+1/2,j} = E_x|^{n}_{i+1/2,j} + \frac{\Delta t}{\epsilon_0 \Delta y}\left[\left(H_z|^{n+1/2}_{i+1/2,j+1/2} - H_z|^{n+1/2}_{i+1/2,j-1/2}\right) - \frac{1}{2}\left[J_x|^{n+1/2}_{i+1/2,j+1/2} + J_x|^{n+1/2}_{i+1/2,j-1/2}\right)\Delta y\right], \quad (14)$$

$$E_y|^{n+1}_{i,j+1/2} = E_y|^{n}_{i,j+1/2} - \frac{\Delta t}{\epsilon_0 \Delta x}\left[\left(H_z|^{n+1/2}_{i+1/2,j+1/2} - H_z|^{n+1/2}_{i-1/2,j+1/2}\right) - \frac{1}{2}\left[J_y|^{n+1/2}_{i+1/2,j+1/2} + J_y|^{n+1/2}_{i-1/2,j+1/2}\right)\Delta y\right], \quad (15)$$

$$H_z|^{n+1/2}_{i+1/2,j+1/2} = H_z|^{n-1/2}_{i+1/2,j+1/2} - \frac{\Delta t}{\mu_0 \Delta x}\left(E_y|^{n}_{i+1,j+1/2)} - E_y|^{n}_{i,j+1/2)}\right) + \frac{\Delta t}{\mu_0 \Delta y}\left(E_x|^{n}_{i+1/2,j+1)} - E_y|^{n}_{i+1/2,j)}\right) - \frac{2\Delta t}{\mu_0}\left(K_z|^{n}_{i+1/2,j+1/2}\right), \quad (16)$$

$$K_z|^{n+1}_{i+1/2,j+1/2} = \frac{1 - 0.5\Gamma\Delta t}{1 + 0.5\Gamma\Delta t} K_z|^{n}_{i+1/2,j+1/2} + \frac{\mu_0 \omega_p^2 \Delta t}{1 + 0.5\Gamma\Delta t} H_z|^{n+1/2}_{i+1/2,j+1/2}, \quad (17)$$

$$J_x|^{n+3/2}_{i+1/2,j+1/2} = \frac{1 - 0.5\Gamma\Delta t}{1 + 0.5\Gamma\Delta t} J_x|^{n+1/2}_{i+1/2,j+1/2} + \frac{1}{2}\frac{\epsilon_0 \omega_p^2 \Delta t}{1 + 0.5\Gamma\Delta t}\left[E_x|^{n+1}_{i+1/2,j+1/2} + E_x|^{n+1}_{i+1/2,j-1/2}\right], \quad (18)$$

$$J_y|^{n+3/2}_{i+1/2,j+1/2)} = \frac{1 - 0.5\Gamma\Delta t}{1 + 0.5\Gamma\Delta t} J_y|^{n+1/2}_{i+1/2,j+1/2} + \frac{1}{2}\frac{\epsilon_0 \omega_p^2 \Delta t}{1 + 0.5\Gamma\Delta t}\left[E_y|^{n+1}_{i+1/2,j+1/2} + E_y|^{n+1}_{i-1/2,j+1/2}\right], \quad (19)$$

where Δx and Δy are spatial discretization and Δt is a temporal discretization.

In the RC method, we calculate a convolution integral, represented by Eq. (9), of electric flux density and electric field recursively. For a dispersive medium described by Eq. (1) and (2), we introduce new fields Ψ_D and Ψ_L known as "recursive acumulators". These fields are given by

$$\Psi_{xD}|^{n}_{i+1/2,j} = C_D^{\rho}\Psi_{xD}|^{n-1}_{i+1/2,j} + C_D^{\delta} E_x|^{n}_{i+1/2,j}, \quad (20)$$

$$\Psi_{yD}|^{n}_{i,j+1/2} = C_D^{\rho}\Psi_{yD}|^{n-1}_{i,j+1/2} + C_D^{\delta} E_y|^{n}_{i,j+1/2}, \quad (21)$$

$$\Psi_{zD}|^{n+1/2}_{i+1/2,j+1/2} = C_D^{\rho}\Psi_{zD}|^{n-1/2}_{i+1/2,j+1/2} + C_D^{\delta} H_z|^{n+1/2}_{i+1/2,j+1/2}, \quad (22)$$

$$\Psi_{xL}|^{n}_{i+1/2,j}(k) = C_{kL}^{\rho}\Psi_{xL}|^{n-1}_{i+1/2,j}(k) + C_{kL}^{\delta} E_x|^{n}_{i+1/2,j}, \quad (23)$$

$$\Psi_{yL}|^{n}_{i,j+1/2}(k) = C_{kL}^{\rho}\Psi_{yL}|^{n-1}_{i,j+1/2}(k) + C_{kL}^{\delta} E_y|^{n}_{i,j+1/2}, \quad (24)$$

$$\Psi_{zL}|^{n+1/2}_{i+1/2,j+1/2}(k) = C_{kL}^{\rho}\Psi_{zL}|^{n-1/2}_{i+1/2,j+1/2}(k) + C_{kL}^{\delta} H_z|^{n+1/2}_{i+1/2,j+1/2}, \quad (25)$$

$$(k = 1, 2, 3, \cdots)$$

where the cofficients C^{ρ}, C^{δ} depend on the cofficients in Eq. (1) and (2).

For the Drude model, these cofficients C_D^{ρ}, C_D^{δ} are defined as

$$C_D^{\rho} = e^{-\Gamma_D \Delta t}, \quad (26)$$

$$C_D^{\delta} = \left(-\frac{\omega_p}{\Gamma_D}\right)^2 (1 - e^{-\Gamma_D \Delta t})^2. \quad (27)$$

For the Lorentz model, C_L^{ρ}, C_L^{δ} are defined as

$$C_{kL}^{\rho} = e^{(-\alpha + i\beta_k)\Delta t}, \quad (28)$$

$$C_{kL}^{\delta} = -i\frac{\gamma_k}{\alpha - i\beta_k}(1 - e^{(-\alpha + i\beta_k)\Delta t})^2, \quad (29)$$

$$(k = 1, 2, 3, \cdots)$$

where $\alpha = \Gamma_L/2$, $\beta_k = \sqrt{\Omega_{kL}^2 - \alpha^2}$, and $\gamma = \Delta\epsilon_k \Omega_{kL}^2/\beta_k$.

Thus, the difference equations in the RC method are written as

$$E_x|^{n+1}_{i+1/2,j)} = C_\alpha E_x|^{n}_{i+1/2,j} + C_\beta\left[H_z|^{n+1/2}_{i+1/2,j+1/2} - H_z|^{n+1/2}_{i+1/2,j-1/2}\right] + C_\gamma\left[\Psi_{xD}|^{n}_{i+1/2,j} + \sum_k \Psi_{xL}|^{n}_{i+1/2,j}(k)\right], \quad (30)$$

$$E_y|^{n+1}_{i,j+1/2} = C_\alpha E_y|^{n}_{i,j+1/2} + C_\beta\left[H_z|^{n+1/2}_{i+1/2,j+1/2} - H_z|^{n+1/2}_{i-1/2,j+1/2}\right] - C_\gamma\left[\Psi_{yD}|^{n}_{i,j+1/2} + \sum_k \Psi_{yL}|^{n}_{i,j+1/2}(k)\right], \quad (31)$$

$$
\begin{aligned}
H_z|^{n+1/2}_{i+1/2,j+1/2} = & C_\alpha H_z|^{n-1/2}_{i+1/2,j+1/2} \\
& -C_\beta \left[E_y|^n_{i+1,j+1/2} - E_y|^n_{i,j+1/2} \right] \\
& +C_\beta \left[E_x|^n_{i+1/2,j+1} - E_x|^n_{i+1/2,j} \right] \\
+C_\gamma & \left[\Psi_{zD}|^{n-1/2}_{i+1/2,j+1/2} + \sum_k \Psi_{zL}|^{n-1/2}_{i+1/2,j+1/2}(k) \right] \quad (32)
\end{aligned}
$$

$$(k = 1, 2, 3, \cdots)$$

In addition, we define χ^0 as

$$\chi^0 = \chi^0_D + Re\left(\sum_k \chi^0_L(k) \right), \quad (33)$$

where

$$\chi^0_D = -\left(\frac{\omega_D}{\gamma_D} \right)^2 (1 - e^{-\gamma_D \Delta t}), \quad (34)$$

$$\chi^0_{kL} = -i \frac{\gamma_k}{\alpha - i\beta_k} (1 - e^{(-\alpha + i\beta_k)\Delta t}). \quad (35)$$

$$(k = 1, 2, 3, \cdots)$$

The last cofficients are defined as

$$C^\alpha = \frac{\epsilon_\infty}{\epsilon_\infty + \chi_0 + \sigma_D \Delta t}, \quad (36)$$

$$C^\beta = \frac{\Delta t}{\Delta x \epsilon_0 (\epsilon_\infty + \chi_0 + \sigma_D \Delta t)}, \quad (37)$$

$$C^\gamma = \frac{1}{\epsilon_\infty + \chi_0 + \sigma_D \Delta t}. \quad (38)$$

REFERENCES

[1] J. B. Pendry: Phys. Rev. Lett. **85** (2000) 3966-3969.

[2] R. W. Ziolkowski: Phys. Rev. E. **64** (2001) 056625-1-056625-15.

[3] Z. Liu, H. Lee, Y. Xiong, C. Sun and X. Zhang: Science **315** (2007) 1686.

[4] J. B. Pendry and D. R. Smith: Physics Today (2004) 37-43.

[5] J. Valentine, S. Zhang, T. Zentgraf, E. Ulin-Avila, D. A. Genov, G. Bartal and X. Zhang: Nature (2008) 07247-1-07247-5.

[6] A. Vial, A.-S. Grimault, D. Macias, D. Barchiesi and M. Lamy: Phys. Rev. B. **71** (2005) 085416-1-085416-5.

[7] P. B. Johnson and R. W. Christy: Phys. Rev. B. **85** Vol**6** 12 (1972) 4370-4379.

[8] U. Kreibig and M. Vollmer: *Optical Properties of Metal Clusters* (Springer Series. in Materials Science, Vol. 25, Springer,. Berlin 1995) pp. 79-99.

[9] U. Kreibig: J. Physics C**2** (1977) 97-103.

[10] A. Taflove and S. C. Hagness: *Computational Electrodynamics: The Finite-Difference Time-Domain Mtehod* (Artech House, Inc., Norwood, MA, 2003) pp. 361-368.

[11] T. Uno: *Finite Difference Time Domain Method for Electromagnetic Field and Antennas* (Corona Publishing CO., LTD, JP, 2000) pp.194-208.

[12] K.-M. Chae, H.-H. Lee, S.-Y. Yim and S.-H. Park: Opt. Express **12** (2004) 2870-2879.